EARTHQUAKE ENGINEERING AND STRUCTURAL DYNAMICS
Earthquake Engng Struct. Dyn. 2001; **30**:1857–1878 (DOI: 10.1002/eqe.98)

Modal identification of structures from ambient vibration, free vibration, and seismic response data via a subspace approach

C. S. Huang[1,*,†] and H. L. Lin[2]

[1]*Department of Civil Engineering, National Chiao Tung University, 1001 Ta-Hseuh Road, Hsinchu 30050, Taiwan*
[2]*Department of Civil Engineering, Tamkang University, Tamsui 25137, Taiwan*

SUMMARY

This work presents a unified procedure for determining the natural frequencies, modal damping ratios and modal shapes of a structure from its ambient vibration, free vibration and earthquake response data. To evaluate the coefficient matrices of a state-space model, the proposed procedure applies a subspace approach cooperating with an instrumental variable concept. The dynamic characteristics of a structure are determined from the coefficient matrices. The feasibility of the procedure is demonstrated through processing an *in situ* ambient vibration measurement of a five-storey steel frame, an impulse response measurement of a three-span continuous bridge, and simulated earthquake responses of five-storey steel frames from shaking table tests. The excellent agreement of the results obtained herein with those published previously confirms the feasibility of the present procedure. Copyright © 2001 John Wiley & Sons, Ltd.

KEY WORDS: system identification; subspace approach; ambient vibration; free vibration; earthquake response

1. INTRODUCTION

Investigating the dynamic characteristics of an existing structure system based on field tests is essential in confirming the construction quality, validating or improving analytical finite element structural models, or conducting damage assessment. To accomplish this task, the popular field tests are ambient vibration tests, forced vibration tests, free vibration tests, and

* Correspondence to: C. S. Huang, Department of Civil Engineering, National Chiao Tung University, 1001 Ta-Hseuh Road, Hsinchu 30050, Taiwan.
† E-mail: cshuang@cc.nctu.edu.tw

Contract/grant sponsor: National Science Council, R.O.C.; contract/grant number: NSC89-2211-E-009-094

Received 13 October 2000
Revised 9 April 2001
Accepted 10 April 2001

earthquake response measurement. Notably, excluding forced vibration tests due to their periodic characteristics of input, identifying the dynamic characteristics of a structural system from the other three tests can be accomplished in time domain.

Even in the time-domain analysis, various schemes are often applied to process the data from various field tests. For example, to determine the dynamic characteristics of a structural system from free vibration test, Ibrahim time-domain system identification (ITD) technique is often applied [1]. However, it cannot be directly applied to process either the ambient vibration test or the earthquake response measurement. That is, to process the ambient vibration measurement, the ITD technique has to comply with random decrement technique [2]. There is no rigorous procedure to extract free vibration responses from earthquake responses such that ITD technique can be applied to determine the dynamic characteristics from the resultant responses. Based on the assumption of stationary process for observed data, time series models, i.e. AR and ARMA models, are also often employed for ambient vibration measurements [3–6]. Apparently, however, this assumption is not valid for free vibration measurement and earthquake response measurement. Consequently, to analyze the observed data from different tests, various techniques as well as the corresponding theoretical backgrounds must be understood, which becomes burdensome for the users. Therefore, this study develops a system identification procedure capable of processing the measurement from various tests.

The proposed procedure is based on state-space model cooperating with a subspace approach. Rao and Arun [7] provided a comprehensive review on the data processing by using state-space approaches, while Van DerVeen *et al.* [8] collected more than 100 articles on signal analysis by subspace-based approaches. Viberg [9] also reviewed and compared numerous subspace-based schemes. He classified these schemes into two categories: (1) realization-based subspace methods [10–12], which estimate the coefficient matrices of a state-space model via measured impulse response functions; (2) direct subspace-based methods [13–16], which estimate the coefficient matrices via observed input and output signals. Apparently, even in the subspace-based approach, varying schemes were applied to the data from varying tests.

To identify the dynamic characteristics of structures from the ambient vibration, free vibration, and earthquake response data, this study develops a unified procedure by extending, with some modification, the direct subspace-based method with the instrumental variables proposed by Viberg *et al.* [17], who developed a procedure to estimate the observability matrix for the state-space model with measured inputs. Furthermore, to demonstrate the feasibility of the proposed procedure, the procedure is applied to process an ambient vibration measurement of a five-storey steel frame, a free vibration measurement of a three-span continuous prestressed concrete bridge, and simulated earthquake responses of two five-storey steel frames from the shaking table test. The dynamic characteristics identified herein are compared with those obtained from other methods.

2. METHODOLOGY

2.1. The relationship between equations of motion and state-space model

The equations of motion for a structural system with n degrees of freedom are

$$\mathbf{M}\ddot{\mathbf{x}} + \mathbf{C}\dot{\mathbf{x}} + \mathbf{K}\mathbf{x} = \mathbf{f} \tag{1}$$

where **M**, **C**, and **K** are the mass, damping and stiffness matrices of the structural system, respectively. They are $n \times n$ matrices. The vector of input forces, **f**, is a column vector with n components. By defining a state variable $\mathbf{z} = (\mathbf{x}^{\mathrm{T}}\dot{\mathbf{x}}^{\mathrm{T}})^{\mathrm{T}}$, the solution for Equation (1) can be expressed as

$$\mathbf{z}(t) = \mathrm{e}^{\mathbf{A}t}\mathbf{z}_0 + \int_0^t \mathrm{e}^{\mathbf{A}(t-\tau)}\hat{\mathbf{f}}(\tau)\,\mathrm{d}\tau \tag{2}$$

where

$$\mathbf{A} = -\mathbf{G}^{-1}\begin{bmatrix} K & \mathbf{0} \\ \mathbf{0} & -M \end{bmatrix} \tag{3a}$$

$$\hat{\mathbf{f}} = \mathbf{G}^{-1}\begin{Bmatrix} \mathbf{f} \\ \mathbf{0} \end{Bmatrix} \tag{3b}$$

$$\mathbf{G} = \begin{bmatrix} \mathbf{C} & \mathbf{M} \\ \mathbf{M} & \mathbf{0} \end{bmatrix} \tag{3c}$$

and $\mathbf{z}_0$ is the initial condition vector. From Equation (2), the solution can be rewritten in the following form:

$$\mathbf{z}(t+\Delta t) = \mathrm{e}^{\mathbf{A}\Delta t}\mathbf{z}(t) + \int_t^{t+\Delta t} \mathrm{e}^{\mathbf{A}(t+\Delta t-\tau)}\hat{\mathbf{f}}(\tau)\,\mathrm{d}\tau \tag{4}$$

where Δt is a time increment. When Δt is sufficiently small, it is reasonable to assume that $\hat{\mathbf{f}}(\tau)$ is a constant vector for τ varying from t to $t+\Delta t$. Then, from Equation (4), the following discrete-time domain model can be obtained:

$$\tilde{\mathbf{z}}_{k+1} = \tilde{\mathbf{A}}\tilde{\mathbf{z}}_k + \tilde{\mathbf{B}}\tilde{\mathbf{f}}_k \tag{5}$$

where

$$\tilde{\mathbf{A}} = \mathrm{e}^{\mathbf{A}\Delta t} \tag{6a}$$

$$\hat{\mathbf{B}} = [\hat{\mathbf{B}}_1 \quad \hat{\mathbf{B}}_2] = \int_{k\Delta t}^{(k+1)\Delta t} \mathrm{e}^{\mathbf{A}((k+1)\Delta t-\tau)}\mathbf{G}^{-1}\,\mathrm{d}\tau \tag{6b}$$

$\tilde{\mathbf{B}} = \hat{\mathbf{B}}_1$, which is a $2n \times n$ matrix, $\tilde{\mathbf{z}}_k = \mathbf{z}(k\Delta t)$, and $\tilde{\mathbf{f}}_k = \mathbf{f}(k\Delta t)$.

When the observed degrees of freedom (l) are less than twice of the total degrees of freedom ($2n$), and when the observed responses are displacement or velocity, at $t = k\Delta t$ the observed responses ($\mathbf{y}_k$) can be expressed as

$$\mathbf{y}_k = \mathbf{L}\tilde{\mathbf{z}}_k + \mathbf{a}_k \tag{7}$$

where **L** is a matrix of selecting observed degrees of freedom with components equal to 0 or 1; $\mathbf{a}_k = \mathbf{a}(k\Delta t)$, a vector of measurement noise, and $\mathbf{a}(t)$ is assumed to be a white noise

process with zero mean. However, if the observed responses are noisy acceleration, then, through Equation (1), the following develops:

$$\mathbf{y}_k = \tilde{\mathbf{E}}\tilde{\mathbf{z}}_k + \tilde{\mathbf{D}}\tilde{\mathbf{f}}_k + \mathbf{a}_k \tag{8}$$

where

$$\tilde{\mathbf{E}} = \tilde{\mathbf{L}}[-\mathbf{M}^{-1}\mathbf{K} \quad -\mathbf{M}^{-1}\mathbf{C}] \tag{9a}$$

$$\tilde{\mathbf{D}} = \tilde{\mathbf{L}}\mathbf{M}^{-1} \tag{9b}$$

and $\tilde{\mathbf{L}}$ is also a matrix of selecting observed degrees of freedom.

Equations (5) and (7) or (8) construct a state-space model. Generally, the state-space model considered in the following will be presented as

$$\tilde{\mathbf{z}}_{k+1} = \tilde{\mathbf{A}}\tilde{\mathbf{z}}_k + \tilde{\mathbf{B}}\tilde{\mathbf{f}}_k + \mathbf{w}_k \tag{10}$$

$$\mathbf{y}_k = \tilde{\mathbf{E}}\tilde{\mathbf{z}}_k + \tilde{\mathbf{D}}\tilde{\mathbf{f}}_k + \mathbf{a}_k \tag{8}$$

where $\mathbf{w}_k = \mathbf{w}(k\Delta t)$, and $\mathbf{w}(t)$ is also a white noise process with zero mean, but is not correlated with $\mathbf{a}(t)$. Notably, when the observed responses are displacement or velocity, $\tilde{\mathbf{E}}$ and $\tilde{\mathbf{D}}$ are equal to $\mathbf{L}$ and $\mathbf{0}$, respectively. In processing the ambient vibration measurement, $\tilde{\mathbf{f}}_k$ is set equal to zero and the input is assumed to the white-noise process $\mathbf{w}(t)$. In processing the measurements from free vibration tests, $\tilde{\mathbf{f}}_k$ and $\mathbf{w}_k$ are equal to zero, simultaneously. When earthquake responses are being considered, $\mathbf{w}_k$ can be set equal to zero.

2.2. Estimation of coefficient matrices

From Equations (10) and (8), one can construct

$$\mathbf{y}_{k+s} = \tilde{\mathbf{E}}\tilde{\mathbf{A}}^s\tilde{\mathbf{z}}_k + \tilde{\mathbf{D}}\tilde{\mathbf{f}}_{k+s} + \sum_{i=1}^{s}\tilde{\mathbf{E}}\tilde{\mathbf{A}}^{i-1}\tilde{\mathbf{B}}\tilde{\mathbf{f}}_{k+s+i-1} + \sum_{i=1}^{s}\tilde{\mathbf{E}}\tilde{\mathbf{A}}^{i-1}\mathbf{w}_{k+s+i-1} + \mathbf{a}_{k+s} \tag{11}$$

Via Equation (11), one can further construct

$$\bar{\mathbf{y}}_k = \mathbf{\Gamma}_\alpha\tilde{\mathbf{z}}_k + \mathbf{\Phi}_\alpha\bar{\mathbf{f}}_k + \bar{\boldsymbol{\delta}}_k \tag{12}$$

where

$$\bar{\mathbf{y}}_k = (\mathbf{y}_k^{\mathrm{T}} \quad \mathbf{y}_{k+1}^{\mathrm{T}} \quad \cdots \quad \mathbf{y}_{k+s-1}^{\mathrm{T}})^{\mathrm{T}} \tag{13a}$$

$$\mathbf{\Gamma}_\alpha = \begin{bmatrix} \tilde{\mathbf{E}} \\ \tilde{\mathbf{E}}\tilde{\mathbf{A}} \\ \vdots \\ \tilde{\mathbf{E}}\tilde{\mathbf{A}}^{s-1} \end{bmatrix} \tag{13b}$$

$$\mathbf{\Phi}_\alpha = \begin{bmatrix} \tilde{\mathbf{D}} & \mathbf{0} & \mathbf{0} & \cdots & \mathbf{0} \\ \tilde{\mathbf{E}}\tilde{\mathbf{B}} & \tilde{\mathbf{D}} & \mathbf{0} & \cdots & \mathbf{0} \\ \tilde{\mathbf{E}}\tilde{\mathbf{A}}\tilde{\mathbf{B}} & \tilde{\mathbf{E}}\tilde{\mathbf{B}} & \tilde{\mathbf{D}} & \cdots & \mathbf{0} \\ \vdots & \vdots & \vdots & \cdots & \vdots \\ \tilde{\mathbf{E}}\tilde{\mathbf{A}}^{s-1}\tilde{\mathbf{B}} & \tilde{\mathbf{E}}\tilde{\mathbf{A}}^{s-2}\tilde{\mathbf{B}} & \tilde{\mathbf{E}}\tilde{\mathbf{A}}^{s-3}\tilde{\mathbf{B}} & \cdots & \tilde{\mathbf{D}} \end{bmatrix} \tag{13c}$$

$$\bar{\mathbf{f}}_k = (\tilde{\mathbf{f}}_k^{\mathrm{T}} \quad \tilde{\mathbf{f}}_{k+1}^{\mathrm{T}} \quad \cdots \quad \tilde{\mathbf{f}}_{k+s-1}^{\mathrm{T}})^{\mathrm{T}} \tag{13d}$$

$$\bar{\boldsymbol{\delta}}_k = \mathbf{\Psi}_\alpha \bar{\mathbf{w}}_k + \bar{\mathbf{a}}_k \tag{13e}$$

$$\mathbf{\Psi}_\alpha = \begin{bmatrix} \mathbf{I} & \mathbf{0} & \mathbf{0} & \cdots & \mathbf{0} \\ \tilde{\mathbf{E}} & \mathbf{I} & \mathbf{0} & \cdots & \mathbf{0} \\ \tilde{\mathbf{E}}\tilde{\mathbf{A}} & \tilde{\mathbf{E}} & \mathbf{I} & \cdots & \mathbf{0} \\ \vdots & \vdots & \vdots & \cdots & \vdots \\ \tilde{\mathbf{E}}\tilde{\mathbf{A}}^{s-2} & \tilde{\mathbf{E}}\tilde{\mathbf{A}}^{s-3} & \tilde{\mathbf{E}}\tilde{\mathbf{A}}^{s-4} & \cdots & \mathbf{I} \end{bmatrix} \tag{13f}$$

$$\bar{\mathbf{w}}_k = (\mathbf{w}_k^{\mathrm{T}} \quad \mathbf{w}_{k+1}^{\mathrm{T}} \quad \cdots \quad \mathbf{w}_{k+s-1}^{\mathrm{T}})^{\mathrm{T}} \tag{13g}$$

$$\bar{\mathbf{a}}_k = (\mathbf{a}_k^{\mathrm{T}} \quad \mathbf{a}_{k+1}^{\mathrm{T}} \quad \cdots \quad \mathbf{a}_{k+s-1}^{\mathrm{T}})^{\mathrm{T}} \tag{13h}$$

and Γ_α is the so-called observability matrix. Viberg [9] suggested that in Equations (13a)–(13h), s should be larger than $2n$. From Equation (12), the following relation can be established:

$$\bar{\mathbf{Y}}_k = \mathbf{\Gamma}_\alpha \bar{\mathbf{Z}}_k + \mathbf{\Phi}_\alpha \bar{\mathbf{F}}_k + \bar{\mathbf{\Delta}}_k \tag{14}$$

where

$$\bar{\mathbf{Y}}_k = [\bar{\mathbf{y}}_k \quad \bar{\mathbf{y}}_{k+1} \quad \cdots \quad \bar{\mathbf{y}}_{k+N-1}] \tag{15a}$$

$$\bar{\mathbf{Z}}_k = [\tilde{\mathbf{z}}_k \quad \tilde{\mathbf{z}}_{k+1} \quad \cdots \quad \tilde{z}_{k+N-1}] \tag{15b}$$

$$\bar{\mathbf{F}}_k = [\bar{\mathbf{f}}_k \quad \bar{\mathbf{f}}_{k+1} \quad \cdots \quad \bar{\mathbf{f}}_{k+N-1}] \tag{15c}$$

$$\bar{\mathbf{\Delta}}_k = [\bar{\boldsymbol{\delta}}_k \quad \bar{\boldsymbol{\delta}}_{k+1} \quad \cdots \quad \bar{\boldsymbol{\delta}}_{k+N-1}] \tag{15d}$$

From linear algebra, one can define an orthogonal projection matrix, $\mathbf{\Pi}_f^\perp$, onto the null-space of $\bar{\mathbf{F}}_k$ as

$$\mathbf{\Pi}_f^\perp = \mathbf{I} - \bar{\mathbf{F}}_k^{\mathrm{T}} (\bar{\mathbf{F}}_k \bar{\mathbf{F}}_k^{\mathrm{T}})^{-1} \bar{\mathbf{F}}_k \tag{16}$$

Multiplying with $\mathbf{\Pi}_f^{\perp}$ on both sides of Equation (14) yields

$$\bar{\mathbf{Y}}_k \mathbf{\Pi}_f^{\perp} = \mathbf{\Gamma}_\alpha \bar{\mathbf{Z}}_k \mathbf{\Pi}_f^{\perp} + \bar{\mathbf{\Delta}}_k \mathbf{\Pi}_f^{\perp} \tag{17}$$

Notably, from Equation (13e), $\bar{\boldsymbol{\delta}}_k$ consists of white noises $\mathbf{w}_m$ and $\mathbf{a}_m$ with $m \geqslant k$. Consequently, it is reasonable to assume that $\bar{\mathbf{f}}_k$ and $\bar{\boldsymbol{\delta}}_t$ are uncorrelated for all k and t, and that $\bar{\mathbf{y}}_m$ and $\bar{\boldsymbol{\delta}}_k$ are uncorrelated for $k > m$. That is

$$E[\bar{\boldsymbol{\delta}}_k \bar{\mathbf{f}}_t^{\mathrm{T}}] = \mathbf{0} \quad \text{for all } k \text{ and } t \tag{18a}$$

$$E[\bar{\boldsymbol{\delta}}_k \bar{\mathbf{y}}_m^{\mathrm{T}}] = \mathbf{0} \quad \text{for } k > m \tag{18b}$$

where $E[\,]$ is a mean value operation.

Introduce instrumental variables, $\mathbf{P}$, defined as

$$\mathbf{P} = \begin{bmatrix} \bar{\mathbf{F}}_p \\ \bar{\mathbf{Y}}_p \end{bmatrix} \tag{19}$$

where $p < k$. Multiplying with $(1/N)\mathbf{P}^{\mathrm{T}}$ on both sides of Equation (17) and employing Equations (18a) and (18b) produce the following relationship, when N is sufficiently large [17]:

$$\frac{1}{N} \bar{\mathbf{Y}}_k \mathbf{\Pi}_f^{\perp} \mathbf{P}^{\mathrm{T}} = \frac{1}{N} \mathbf{\Gamma}_\alpha \bar{\mathbf{Z}}_k \mathbf{\Pi}_f^{\perp} \mathbf{P}^{\mathrm{T}} \tag{20}$$

One may multiply with weighting matrices, $\mathbf{W}_r$ and $\mathbf{W}_c$, on both sides of Equation (20), which produces

$$\frac{1}{N} \mathbf{W}_r \bar{\mathbf{Y}}_k \mathbf{\Pi}_f^{\perp} \mathbf{P}^{\mathrm{T}} \mathbf{W}_c = \frac{1}{N} \mathbf{W}_r \mathbf{\Gamma}_\alpha \bar{\mathbf{Z}}_k \mathbf{\Pi}_f^{\perp} \mathbf{P}^{\mathrm{T}} \mathbf{W}_c \tag{21}$$

where $\mathbf{W}_r$ must be a positive matrix and the rank of $\mathbf{W}_c$ must be not smaller than $2n$ [18]. The weighting matrices may influence the variance of the estimated coefficient matrices of Equations (8) and (10) due to noise and the bias of the estimation due to under-modelling [18, 19]. In the following, the weighting matrices suggested by Verhaegen [15] are chosen:

$$\mathbf{W}_r = \mathbf{I}, \tag{22a}$$

$$\mathbf{W}_c = \left(\frac{1}{N} \mathbf{P} \mathbf{\Pi}_f^{\perp} \mathbf{P}^{\mathrm{T}} \right)^{-1/2} \tag{22b}$$

Define a matrix $\bar{\mathbf{H}}$ equal to the left-hand side of Equation (21). That is

$$\bar{\mathbf{H}} = \frac{1}{N} \mathbf{W}_r \bar{\mathbf{Y}}_k \mathbf{\Pi}_f^{\perp} \mathbf{P}^{\mathrm{T}} \mathbf{W}_c \tag{23}$$

Via singular value decomposition, the following relation holds:

$$\bar{\mathbf{H}} \approx \mathbf{Q}_{\bar{n}} \sum\nolimits_{\bar{n}} \mathbf{V}_{\bar{n}}^{\mathrm{T}} \tag{24}$$

where $\sum_{\bar{n}}$ is a diagonal matrix containing the $\bar{n}$ largest singular values, the columns of $\mathbf{Q}_{\bar{n}}$ and $\mathbf{V}_{\bar{n}}$ are the corresponding left and right singular vectors, respectively. Notably, in the perfect data case $\bar{n}$ is equal to $2n$. However, if the data contain noises, $\bar{n}$ is typically larger than $2n$.

Thus, Equations (21), (23), and (24) produce

$$\mathbf{\Gamma}_\alpha = \hat{\mathbf{\Gamma}}_\alpha \mathbf{T}_{\bar{n}} \tag{25}$$

where

$$\hat{\mathbf{\Gamma}}_\alpha = \mathbf{W}_r^{-1} \mathbf{Q}_{\bar{n}}, \tag{26a}$$

$$\mathbf{T}_{\bar{n}} = \sum_{\bar{n}} \bar{\mathbf{V}}_{\bar{n}} \left(\frac{1}{N} \bar{\mathbf{Z}}_k \mathbf{\Pi}_f^{\perp} \mathbf{P}^{\mathrm{T}} \mathbf{W}_c \right)^{-1} \tag{26b}$$

Up to this point in the process, $\hat{\mathbf{\Gamma}}_\alpha$ could be evaluated from Equation (26a) by using the observed responses. However, as $\bar{\mathbf{Z}}_k$ in Equation (26b) is still unknown, $\mathbf{\Gamma}_\alpha$ cannot be evaluated.

Substituting Equation (25) into Equation (12) yields

$$\bar{\mathbf{y}}_k = \hat{\mathbf{\Gamma}}_\alpha \hat{\mathbf{z}}_k + \mathbf{\Phi}_\alpha \bar{\mathbf{f}}_k + \bar{\boldsymbol{\delta}}_k \tag{27}$$

where $\hat{\mathbf{z}}_k = \mathbf{T}_{\bar{n}} \tilde{\mathbf{z}}_k$, which indicates that $\mathbf{T}_{\bar{n}}$ can be treated as a transformation matrix for state-space variables within different bases. As Equation (12) is resulted from Equations (8) and (10), Equation (27), thus, corresponds with the following state-space model:

$$\hat{\mathbf{z}}_{k+1} = \hat{\mathbf{A}} \hat{\mathbf{z}}_k + \hat{\mathbf{B}} \tilde{\mathbf{f}}_k + \mathbf{T}_{\bar{n}} \mathbf{w}_k \tag{28a}$$

$$\mathbf{y}_k = \hat{\mathbf{E}} \hat{\mathbf{z}}_k + \tilde{\mathbf{D}} \tilde{\mathbf{f}}_k + \mathbf{a}_k \tag{28b}$$

where

$$\hat{\mathbf{A}} = \mathbf{T}_{\bar{n}} \tilde{\mathbf{A}} \mathbf{T}_{\bar{n}}^{-1} \tag{29a}$$

$$\hat{\mathbf{B}} = \mathbf{T}_{\bar{n}} \tilde{\mathbf{B}} \tag{29b}$$

$$\hat{\mathbf{E}} = \tilde{\mathbf{E}} \mathbf{T}_{\bar{n}}^{-1} \tag{29c}$$

As the expression of $\mathbf{\Gamma}_\alpha$ was found in Equation (13b), a similar expression for $\hat{\mathbf{\Gamma}}_\alpha$ can be established further:

$$\hat{\mathbf{\Gamma}}_\alpha = \begin{bmatrix} \hat{\mathbf{E}} \\ \hat{\mathbf{E}}\hat{\mathbf{A}} \\ \vdots \\ \hat{\mathbf{E}}\hat{\mathbf{A}}^{s-1} \end{bmatrix} \tag{30}$$

Notably, the above derivation, that is, from Equations (11)–(30), is also valid for $\tilde{\mathbf{f}}_k = \mathbf{0}$, implying that the previous equations are also suitable for processing both the ambient vibration measurement and free vibration measurement. In these instances, $\mathbf{\Pi}_f^{\perp} = \mathbf{I}$.

After $\hat{\mathbf{\Gamma}}_\alpha$ has been determined from the observed data, $\hat{\mathbf{A}}$ and $\hat{\mathbf{E}}$ can be estimated directly as follows:

(a) Establish the following two matrices from the relationship given in Equation (30):

$$\hat{\mathbf{\Gamma}}_{\alpha 1} = \begin{bmatrix} \hat{\mathbf{E}} \\ \hat{\mathbf{E}}\hat{\mathbf{A}} \\ \vdots \\ \hat{\mathbf{E}}\hat{\mathbf{A}}^{s-2} \end{bmatrix} \tag{31a}$$

$$\hat{\mathbf{\Gamma}}_{\alpha 2} = \begin{bmatrix} \hat{\mathbf{E}}\hat{\mathbf{A}} \\ \hat{\mathbf{E}}\hat{\mathbf{A}}^{2} \\ \vdots \\ \hat{\mathbf{E}}\hat{\mathbf{A}}^{s-1} \end{bmatrix} \tag{31b}$$

(b) From Equations (31a) and (31b), one has

$$\hat{\mathbf{\Gamma}}_{\alpha 2} = \hat{\mathbf{\Gamma}}_{\alpha 1}\hat{\mathbf{A}} \tag{32}$$

Consequently,

$$\hat{\mathbf{A}} = \hat{\mathbf{\Gamma}}_{\alpha 1}^{+}\hat{\mathbf{\Gamma}}_{\alpha 2} \tag{33}$$

where the subscript '+' denotes the generalized inverse operation for a matrix. The solution given by Equation (33) is the least-squares error solution for Equation (32).

(c) From the relationship provided by Equation (30), one can also establish the following equation:

$$\hat{\mathbf{E}}\hat{\mathbf{\Omega}} = \hat{\mathbf{\Gamma}}_{\alpha p} \tag{34}$$

where

$$\hat{\mathbf{\Omega}} = [\mathbf{I} \quad \hat{\mathbf{A}} \quad \hat{\mathbf{A}}^2 \quad \cdots \quad \hat{\mathbf{A}}^5] \tag{35a}$$

$$\hat{\mathbf{\Gamma}}_{\alpha p} = [\hat{\mathbf{E}} \quad \hat{\mathbf{E}}\hat{\mathbf{A}} \quad \hat{\mathbf{E}}\hat{\mathbf{A}}^2 \quad \cdots \quad \hat{\mathbf{E}}\hat{\mathbf{A}}^5], \tag{35b}$$

The matrix $\hat{\mathbf{\Gamma}}_{\alpha p}$ is equal to the first six block rows of $\hat{\mathbf{\Gamma}}_\alpha$, and $\hat{\mathbf{\Omega}}$ is established by employing the estimated $\hat{\mathbf{A}}$ from the previous step. It should be noted that the order of 5 for $\hat{\mathbf{A}}$ employed in Equation (35a) was chosen arbitrarily. Since the modulus of the eigenvalues of $\hat{\mathbf{A}}$ is less than

one for a stable dynamic system given by Equation (1), higher order of $\hat{\mathbf{A}}$ can be negligible in estimating $\hat{\mathbf{E}}$. From Equation (34), $\hat{\mathbf{E}}$ can be determined by

$$\hat{\mathbf{E}} = \hat{\mathbf{\Gamma}}_{\alpha p} \hat{\mathbf{\Omega}}^{+} \tag{36}$$

Again, the solution of $\hat{\mathbf{E}}$ provided by Equation (36) is the least-squares error solution for the relationship given by Equation (34).

The estimation for the other coefficient matrices, $\hat{\mathbf{B}}$ and $\tilde{\mathbf{D}}$, is not included herein since they are not related to the determination of the dynamic characteristics of a structural system.

2.3. Determination of dynamic characteristics of a structural system

When the equations of motion, i.e. Equation (1), are expressed in terms of the space-state variable, $\mathbf{z}$, it is well known that the dynamic characteristics of the structural system are determined by the eigenvalues and eigenvectors of $\mathbf{A}$ in Equation (3a). However, $\mathbf{A}$ cannot be determined from the preceding derivation. Thus, to find the dynamic characteristics, $\hat{\mathbf{A}}$ is employed. Equations (6a) and (29) reveal that

$$\hat{\lambda}_j = \mathrm{e}^{\lambda_j \Delta t} \tag{37a}$$

$$\hat{\boldsymbol{\varphi}}_j = \mathbf{T}_{\bar{n}} \boldsymbol{\varphi}_j \tag{37b}$$

where λ_j and $\hat{\lambda}_j$ are the jth eigenvalue of $\mathbf{A}$ and $\hat{\mathbf{A}}$, respectively, while $\boldsymbol{\varphi}_j$ and $\hat{\boldsymbol{\varphi}}_j$ are the corresponding eigenvectors. Apparently, since $\mathbf{T}_{\bar{n}}$ remains unknown, the eigenvectors of $\mathbf{A}$ from Equation (37b) cannot be evaluated. Nevertheless, usually, one only needs to determine the eigenvector (or modal shape) corresponding to the observed degrees of freedom, $\boldsymbol{\varphi}_{j,y}$. From Equation (28b), the following relation can be discovered:

$$\boldsymbol{\varphi}_{j,y} = \hat{\mathbf{E}} \hat{\boldsymbol{\varphi}}_j \tag{38}$$

The eigenvalues are complex numbers. Let

$$\lambda_j = \alpha_j + \mathrm{i}\beta_j \tag{39a}$$

$$\hat{\lambda}_j = a_j + \mathrm{i}b_j \tag{39b}$$

From Equation (37a), one has

$$\alpha_j = \frac{1}{2\Delta t} \ln(a_j^2 + b_j^2) \tag{40a}$$

$$\beta_j = \frac{1}{\Delta t} \tan^{-1}\left(\frac{b_j}{a_j}\right) \tag{40b}$$

Then, the pseudo-undamped circular natural frequency for the system becomes

$$\omega_j = \sqrt{\alpha_j^2 + \beta_j^2} \tag{41a}$$

and the modal damping ratio is

$$\xi_j = -\alpha_j/\omega_j. \tag{41b}$$

In a proportionally damped system, ω_j is equivalent to its undamped circular natural frequency.

3. APPLICATIONS

To demonstrate the feasibility of the proposed procedure on processing the data in real applications, the proposed procedures were applied to identify the dynamic characteristics of structures from their ambient vibration measurement, simulated response data from shaking table tests, and free vibration measurement.

3.1. Application to ambient vibration measurement

To show the validity of applying the identification procedure to ambient vibration measurement, the measured data from a five-storey steel structure were processed. The five-storey steel structure employed herein is a moment-resisting frame, and was built for structural control technique research through full-scale field tests organized by the National Center for Research on Earthquake Engineering (NCREE) in Taiwan. Hence, the structure was designed to be more flexible than a common building is, and contains no walls or bracing. Figure 1 schematically depicts the structure, which consists primarily of four corner columns and four girders that are made of ASTM A36 material.

To measure the ambient vibration of the structure, six velocity-type sensors with very high sensitivity were attached to the appropriate locations. The analogue sensor signals were converted to digital data and recorded in a PC-based portable data acquisition system. The resolution for the entire measuring system can attain a maximum of 10^{-4} cm/sec. In the acquisition system, high- and low-pass filters are included. Notably, their cut-off frequencies were fixed to 0.1 Hz and one-third of sampling rate, respectively.

Owing to the symmetry of the structure and high stiffness of the floor diaphragms, it is reasonable to describe the motion of each floor via three uncoupled degrees of freedom, namely, two translation motions and a torsion motion. Therefore, the responses of the three degrees of freedom for each floor could be independently measured. To measure the translation motion in the y-direction, six sensors were placed at the geometrical centre of each floor, including the footing. The ambient vibration responses were recorded for 10 min with a sampling rate of 100 Hz.

In this application, the input was not measured. Rather, only 5-min recorded responses for the six floors, including the footing, were processed simultaneously. Table I presents the identified results, which corresponded to $\bar{n}$, the number of singular values in Equation (24), which was equal to 18. The results were obtained by increasing $\bar{n}$ until they stably appeared. Figure 2 illustrates the ratios of the singular values over the largest one, which indicates that the ratio corresponding to $\bar{n} = 18$ is close to 0.01, and there is also a sharp decrease in ratios around $\bar{n} = 18$. Hence, the ratio plots for the singular values for $\bar{\mathbf{H}}$ can be helpful to determine what $\bar{n}$ value should be used.

Table I also lists the identified results obtained by employing the multivariate ARMA model in combination with a two-stage least-squares approach [20]. Comparing the present results

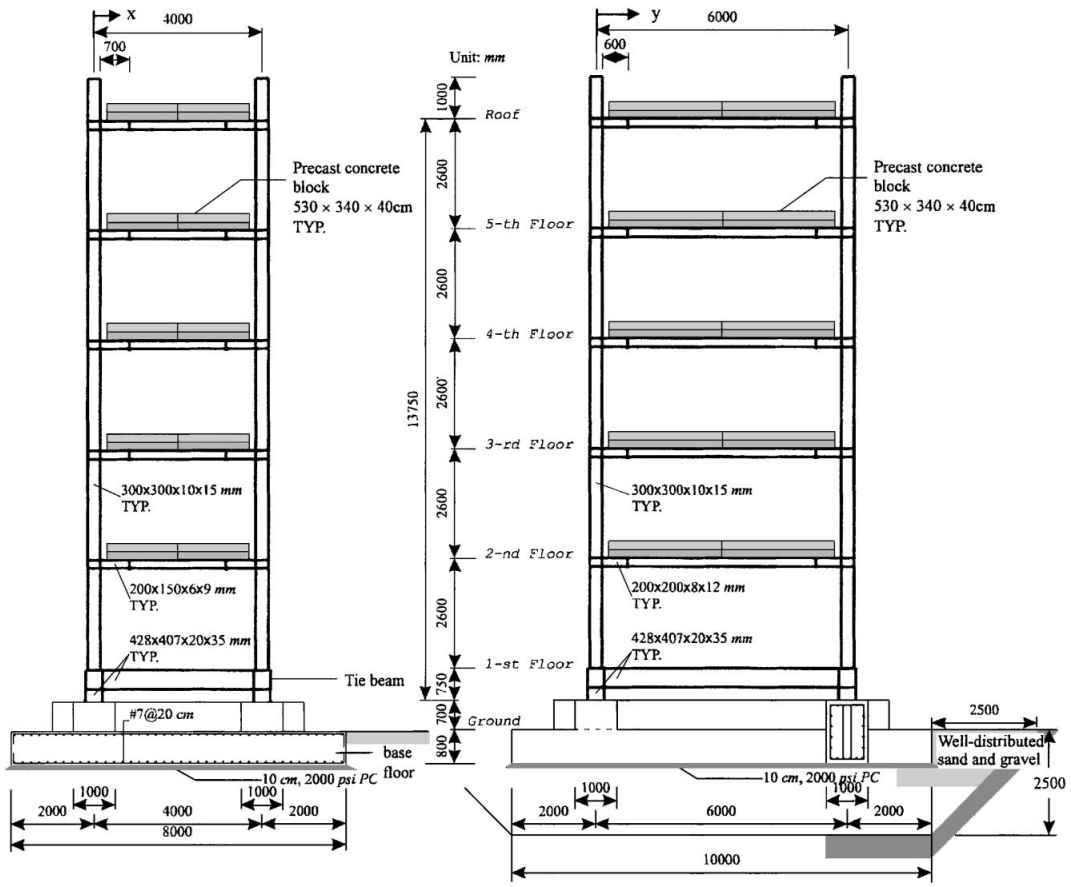

Figure 1. Sketch of a five-storey steel structure.

with those published reveals an excellent agreement between them. Strictly speaking, the agreement for the frequencies and modal shapes is superior to that for the damping ratios.

3.2. Application to simulated earthquake responses from shaking table tests

Shaking table tests are often employed in a laboratory to investigate the behaviours of structures under earthquake. To generate a set of earthquake response data for a benchmark model of a five-storey steel structure, NCREE performed a series of shaking table tests on two steel frames [21] (Figure 3). One steel frame is represented as 'std', which is 3 m long, 2 m wide, and 6.5 m high. Lead blocks were piled on each floor such that the mass for each floor was roughly 3664 kg. A subsequent frame is denoted as 'add_*k*', which is identical to 'std' except that stiffening braces were installed in the fourth storey. The frames were subjected to base excitation of various earthquake records, such as El Centro and Kobe earthquakes with varying reduction levels. Notably, white-noise input was also considered. The

Table I. Identified results from ambient vibration measurement.

Mode	Frequencies (Hz)		Mode shapes		Modal damping (%)	
	Present	ARMAV	Present	ARMAV	Present	ARMAV
1	0.88	0.88	$\begin{Bmatrix} 1.0 \\ 0.85 \\ 0.68 \\ 0.42 \\ 0.15 \\ 0.002 \end{Bmatrix}$	$\begin{Bmatrix} 1.0 \\ 0.85 \\ 0.68 \\ 0.42 \\ 0.16 \\ / \end{Bmatrix}$	0.22	0.27
2	2.93	2.93	$\begin{Bmatrix} -0.88 \\ -0.059 \\ 0.78 \\ 1.0 \\ 0.53 \\ 0.009 \end{Bmatrix}$	$\begin{Bmatrix} -0.88 \\ -0.059 \\ 0.78 \\ 1.0 \\ 0.53 \\ / \end{Bmatrix}$	0.20	0.22
3	5.54	5.55	$\begin{Bmatrix} 0.71 \\ -0.85 \\ -0.81 \\ 0.74 \\ 1.0 \\ 0.019 \end{Bmatrix}$	$\begin{Bmatrix} 0.71 \\ -0.86 \\ -0.80 \\ 0.75 \\ 1.0 \\ / \end{Bmatrix}$	0.51	0.46
4	8.37	8.37	$\begin{Bmatrix} -0.36 \\ 0.98 \\ -0.61 \\ -0.41 \\ 1.0 \\ 0.012 \end{Bmatrix}$	$\begin{Bmatrix} -0.35 \\ 0.96 \\ -0.58 \\ -0.41 \\ 1.0 \\ / \end{Bmatrix}$	0.49	0.52
5	10.4	10.4	$\begin{Bmatrix} -0.15 \\ 0.62 \\ -0.96 \\ 1.0 \\ -0.77 \\ -0.018 \end{Bmatrix}$	$\begin{Bmatrix} -0.16 \\ 0.62 \\ -0.98 \\ 1.0 \\ -0.83 \\ / \end{Bmatrix}$	0.46	0.51

Note: / means no data are available.

displacement, velocity, and acceleration responses of each floor were measured during the tests.

Figure 4(a) depicts time histories for the acceleration responses of the first, third, and fifth floors in long-span direction for frame 'add_k', which was subjected to 8 per cent of Kobe earthquake. Table II summarizes the identified results obtained from the responses for all floors at $t = 7$–20 s and the corresponding input. Due to the insufficient high-frequency components of the input, the fifth mode was not excited significantly and, thus, not identifiable (Figure 4(b)). Thus, to identify all five modes, the responses subjected to white noise excitation and the corresponding input were used for identification. Notably,

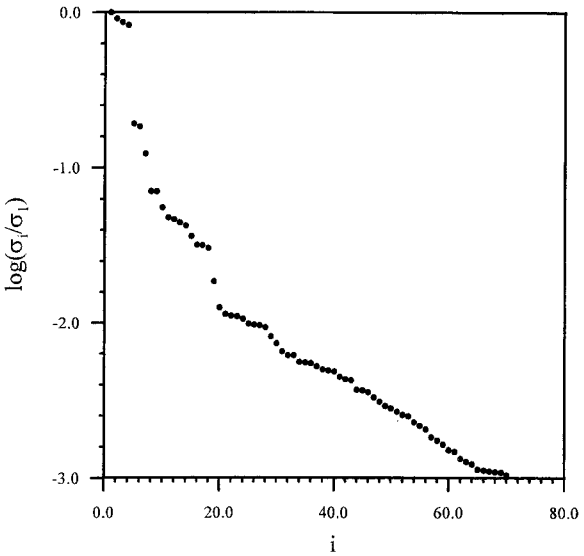

Figure 2. The variation of σ_i/σ_1.

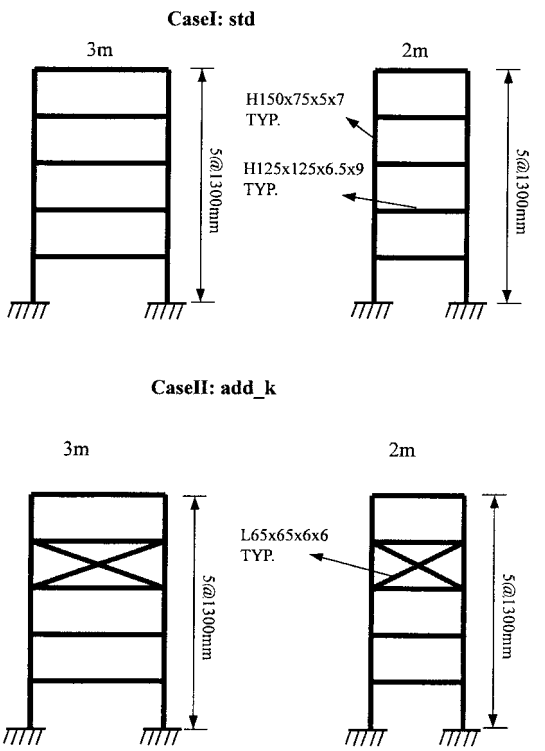

Figure 3. Simple sketch of two five-storey frames.

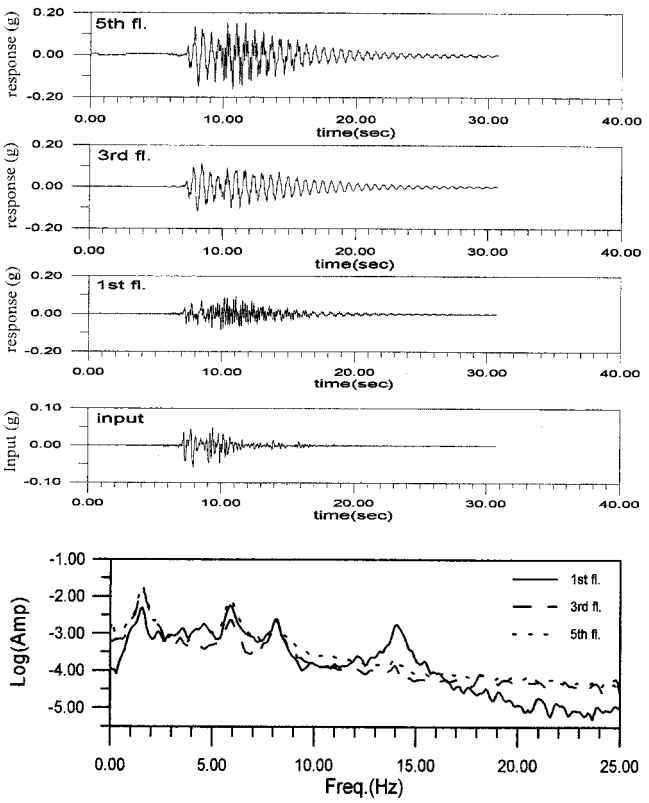

Figure 4. Response of frame "add_k" and the corresponding Fourier spectrum.

the maximum response produced by the white-noise input is approximately 50 per cent less than that produced by 8 per cent of Kobe earthquake input [21]. The identified results are also given in Table II and Figure 5.

For comparison, the identified results of frame 'std' and the analytical results [21] of these two frames are also summarized in Table II and Figure 5. These experimental results were obtained from the input and output responses of frame 'std' subjected to 8 per cent of Kobe earthquake in long-span direction. Via the design data, the analytical results were obtained from commercial finite element package, DRAIN_2D [21].

To evaluate the correlation of mode shapes obtained from different methods and frames, the index of modal assurance criterion (MAC) [22] was computed to indicate the correlation between any two mode shapes of interest, which is defined as

$$\mathrm{MAC}(\boldsymbol{\varphi}_{iI}, \boldsymbol{\varphi}_{iA}) = \frac{|\boldsymbol{\varphi}_{iI}^{\mathrm{T}} \boldsymbol{\varphi}_{iA}|^2}{\boldsymbol{\varphi}_{iI}^{\mathrm{T}} \boldsymbol{\varphi}_{iI} \boldsymbol{\varphi}_{iA}^{\mathrm{T}} \boldsymbol{\varphi}_{iA}} \tag{42}$$

To compare the identified mode shapes with analytical ones for frames 'std' and 'add_k', $\boldsymbol{\varphi}_{iI}$ and $\boldsymbol{\varphi}_{iA}$ represent the ith identified and analytical mode shape, respectively. Table II also lists

Table II. Identified results from shaking table tests.

Frame		std.		add_k		
Method		Present	DRAIN_2D [21]	Present		DRAIN_2D [21]
Input		8% Kobe	None	8% Kobe	White noise	None
Frequency (Hz)	Mode 1	1.40	1.40	1.52	1.53	1.57
	2	4.53	4.54	5.94	5.94	6.14
	3	8.23	8.50	8.22	8.23	8.50
	4	12.39	13.11	14.00	14.01	14.97
	5	15.99	17.14	/	18.46	24.02
Damping ratio (%)	1	1.30		1.90	1.30	
	2	0.16		0.17	0.18	
	3	0.19	/	0.18	0.14	/
	4	0.13		0.18	0.12	
	5	0.10		/	0.30	
MAC	1	1.00		1.00	1.00	
	2	1.00		0.99	0.99	/
	3	1.00	/	0.99	0.09	
	4	1.00		1.00	1.00	
	5	1.00		/	0.97	

Note: / no data are available.

the corresponding MAC value. Apparently, two corresponding modes are well correlated if the MAC value is close to one, and uncorrelated if close to zero.

From the identified results for frame 'add_k' (Table II), it is observed that the identified frequencies and modal shapes from the responses caused by 8 per cent Kobe earthquake input are almost identical with those from the responses caused by white-noise input. It should be noted that the former input produced a maximum response, which was twice as large as that caused by the latter. However, the identified modal damping ratios from the former responses are consistently larger than the latter ones. Comparing the identified results with the analytical ones reveals that the identified frequencies are smaller than the analytical ones, particularly for higher modes. However, the experimental and analytical modal shapes display excellent agreement. Notably, although the first experimental modal damping ratio is close to the typical designed value, 2 per cent, the experimental modal damping ratios for the remainder of the modes are much less than the designed ones.

The identified and analytical results for frame 'std' reveal similar trends to those for frame 'add_k'. Moreover, the experimental frequencies and modal shapes show better agreement with the analytical ones for frame 'std' than for frame 'add_k'.

When comparing the identified results of the two frames listed in Table II, as expected, the frequencies for frame 'std' are smaller than those for frame 'add_k', except for the third mode. The exception can be explained from the corresponding mode shapes (Figure 5). In the third mode shapes for both frames, the modal components for the third and fourth floors are almost identical such that the stiffening braces between the two floors displayed no effect for this particular mode. Interestingly, for the same excitation input, the identified modal damping

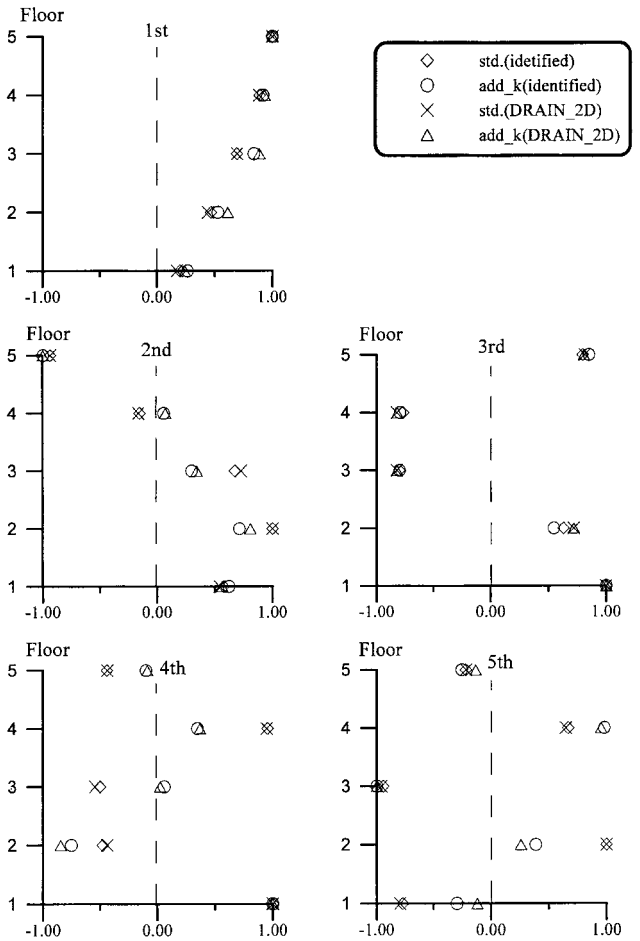

Figure 5. Mode shapes for two steel frames.

ratios for frame 'std' are generally smaller than those for frame 'add_k', although the former frame had responses larger than those of the latter by nearly 20 per cent [21].

To investigate the effect of stiffening braces on the modal shapes, Table III lists MAC values for the identified modal shapes of frame 'add_k' with respect to those of frame 'std'. These values were computed via Equation (42), in which $\boldsymbol{\varphi}_{iI}$ and $\boldsymbol{\varphi}_{iA}$ represent the ith mode shape for frames 'std' and 'add_k', respectively. Since the fifth mode of frame 'add_k' was not identified from the responses for 8 per cent of Kobe earthquake input, Table III presents no corresponding data. The MAC values in Table III indicate that the stiffening braces alter the fourth and fifth modes significantly. Interestingly, the existence of the stiffening braces results in the largest relative frequency variation for the second mode, which would not produce the smallest MAC value.

To further examine the correlation of all mode shapes for the two frames at a common co-ordinate, the index of co-ordinate modal assurance criterion (COMAC) [23] was also adopted

Table III. Comparison of experimental modal shapes for frame 'add_k' with those for frame 'std'.

Mode or floor	MAC		COMAC	
	8% Kobe	White noise	8% Kobe	White noise
1	0.99	0.99	1.00	0.92
2	0.91	0.91	0.90	0.82
3	1.00	1.00	0.74	0.83
4	0.65	0.66	0.83	0.82
5	/	0.76	0.95	0.96

Note: / no data are available.

here. The COMAC for co-ordinate i is defined as

$$\mathrm{COMAC}(i) = \frac{(\sum_{j=1}^{J} \varphi_{s,j}(i)\varphi_{k,j}(i))^2}{\sum_{j=1}^{J} (\varphi_{s,j}(i))^2 \sum_{j=1}^{J} (\varphi_{k,j}(i))^2} \tag{43}$$

where J is the total number of correlated mode pairs, $\varphi_{s,j}(i)$ and $\varphi_{k,j}(i)$ are, respectively, values of experimental mode shape vectors for frames 'std' and 'add_k' in correlated mode j at location i. A value of COMAC close to one suggests a close correlation between the mode shapes for frames 'std' and 'add_k' at location i.

Table III also displays the computed COMAC values. Notably, the COMAC values for the case with 8 per cent of Kobe earthquake input differ significantly from those for the case of white-noise input, as J (in Equation (43)) is equal to 4 for the former case and equal to 5 for the latter case. From the fifth mode shapes shown in Figure 5, the modal components corresponding to the first and second floors vary substantially for the two frames, while the correlating components of the third and fifth floors are very similar. Consequently, the COMAC values for the first and second floors in the case with 8 per cent of Kobe earthquake input are larger than those of white-noise input. However, for the third and fifth floors, the opposite trend is revealed. Apparently, the smallest COMAC value may occur on various floors when different numbers of modes are employed. Nevertheless, the floors corresponding to stiffness change have smaller COMAC values.

3.3. Application to free vibration test

As a third example, to identify the dynamic characteristics of a highway bridge in vertical direction from its impulse test, the proposed procedure was applied. This test was conducted on an elevated highway bridge before it was opened to the public. The bridge consists of three-span continuous pre-stressed concrete box-girders with varying cross-sections and, in total, is 360 m long (Figure 6). Furthermore, the bridge is supported by rollers in the longitudinal direction but is constrained in the transverse and vertical directions at the two far ends. Expansion joints separate both of the two end spans from the adjacent spans.

The impulsive force was imposed near the middle point of the bridge. It was generated by simply allowing the rear wheels of a loaded truck weighing nearly 14 tons to fall down from the top of a concrete block of 20-cm height.

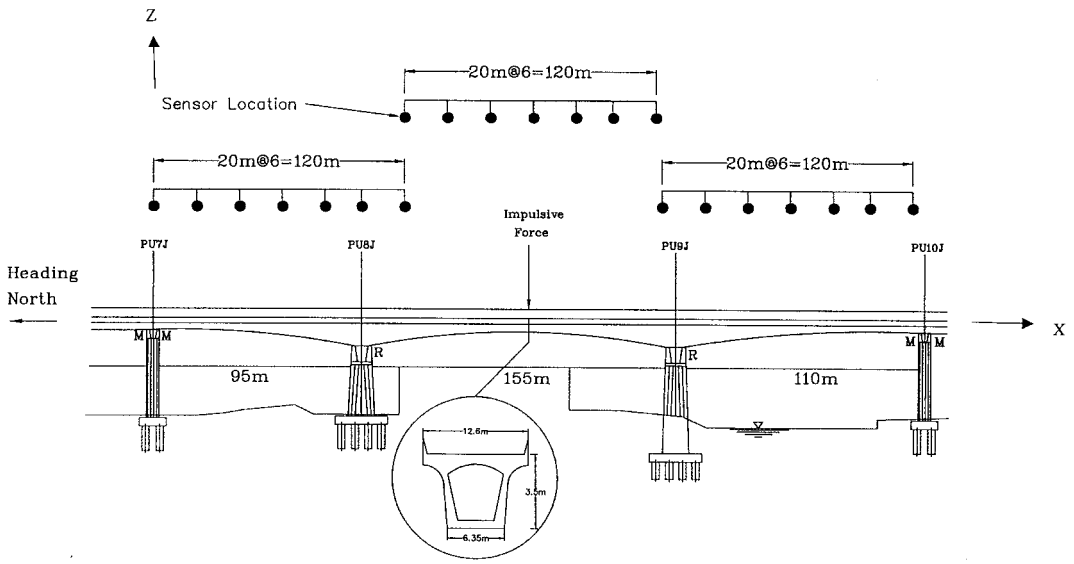

Figure 6. A three-span continuous bridge and sensor layout.

When the force was applied, several highly sensitive sensors of servo velocity type were applied to measure the free vibration response of the bridge. The measuring system was identical to that used for ambient vibration measurement described in Section 3.1. However, at the time of testing, only seven sensors were available, therefore they were deployed in a 20-m interval along the centreline of the bridge (Figure 6). Also, under testing, the bridge was divided into three segments of 120 m. The vertical free vibration responses in each segment caused by an impulsive force were measured in turn with the sensor deployment shown in Figure 6. The responses were recorded for 1 min with a sampling rate of 50 Hz. Notably, the overlapped point for any two adjacent segments was employed to correlate the modal shapes obtained from the three segments.

Figure 7 depicts the free vibration responses in the vertical direction recorded at $x = 40, 180,$ 340 m. The responses that correspond to a long elapsed time (i.e. the response for $t > 40$ s) are primarily the ambient vibration responses. The magnitude of free vibration responses at $x = 340$ m, far from the loading point, is still much larger than that for the ambient vibration responses. Herein, ambient responses are treated as noise. The recorded responses within 5 s after the maximum response occurred were employed for identification analysis.

Table IV summarizes the identified results; it also lists the results of Huang *et al.* [2] via the Ibrahim time-domain system identification (ITD) technique. In total, five modes are identified. Figure 8 shows the identified modal shapes obtained from both methods. Also, Table IV lists the MAC values of the identified modal shapes from these two methods. Evidently, the identified results from the present procedure correspond excellently with those from the ITD technique, especially for the frequencies. However, the identified modal damping ratios herein are somewhat smaller than those from the ITD technique. Figure 8 evidences that the identified modal shapes from the present approach closely correspond to those from the

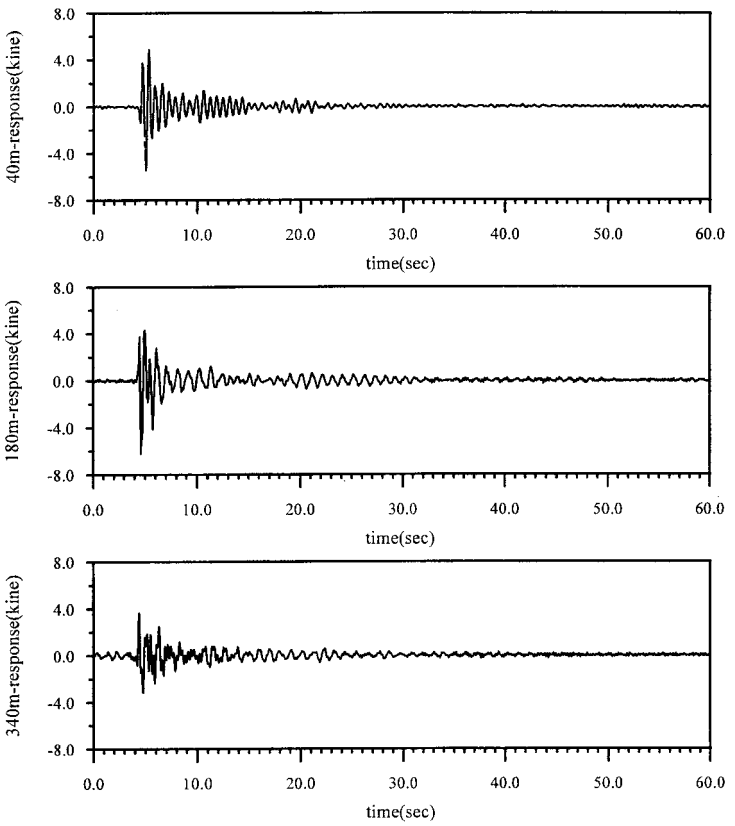

Figure 7. Impact responses at $x = 40, 180$ and 340 m.

Table IV. Identified results of a bridge from impulse tests.

Mode	Frequencies (Hz)		Modal damping (%)		MAC
	Present	ITD [2]	Present	ITD [2]	
1	0.95	0.96	2.4	3.0	1.0
2	1.53	1.52	4.0	5.1	0.96
3	2.17	2.15	5.2	6.6	0.98
4	3.56	3.56	1.5	1.5	1.0
5	4.37	4.36	1.7	1.8	0.93

ITD technique, excluding few modal components of the second and fifth modes. However, judged from the identified modal shapes, our components are more reasonable than those from the ITD technique. In sum, this excellent agreement confirms the applicability of the present approach on processing the free vibration data.

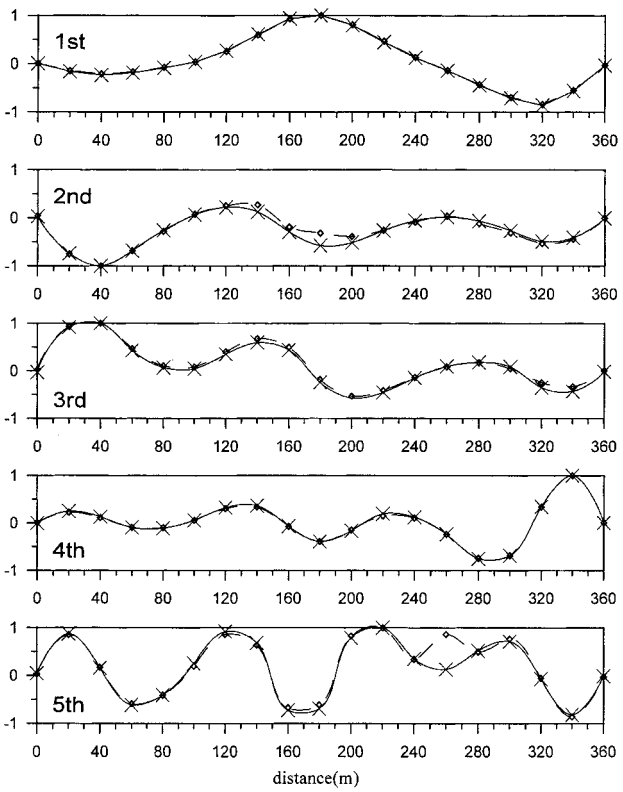

Figure 8. Comparison of identified mode shapes ($-\diamond-$ ITD), ($-\times-$) present.

4. CONCLUDING REMARKS

A unified procedure to identify the dynamic characteristics of the structural system from ambient vibration, free vibration, and earthquake response data has been presented herein. This procedure was established through a state-space model to describe the measured responses. The coefficient matrices related to the dynamic characteristics were evaluated by a subspace method co-operating with the concept of instrumental variable. Then, the dynamic characteristics were evaluated from the eigenvalues and eigenvectors of a coefficient matrix. One of the primary advantages of the procedure is that it proposes a suitable order for the state-space model from the singular values of $\bar{H}$ in Equation (23).

To demonstrate its feasibility for actual applications, the proposed procedure has been applied to process *in situ* ambient vibration measurement of a five-storey steel frame and free vibration measurement of a three-span continuous highway bridge. The identified dynamic characteristics from the ambient vibration data closely corresponded to those obtained from the multivariate ARMA model with a two-stage least-squares approach. The identified results from the free vibration data also display an excellent agreement with those from the ITD technique, thus validating the applicability of the proposed approach.

The proposed procedure was also applied to process the simulated earthquake responses of acceleration from shaking table tests of two five-storey steel frames. Comparison of the experimental results with the finite element solution reveals a superior match for all of the modal shapes and frequencies of lower modes. Comparison of the identified dynamic characteristics for these two frames also reveals that the frame with stiffening braces at the fourth storey has significantly different shapes of the fourth and fifth modes from those for the frame without braces.

Finally, it is believed that the proposed procedure can be successfully applied to process real earthquake responses of a structure despite the fact that the real earthquake response measurement is more complicated than that from shaking table test.

ACKNOWLEDGEMENTS

The work reported herein was supported by the National Science Council, R.O.C. through research grant no. NSC89-2211-E-009-094. This support is gratefully acknowledged. Appreciation is also extended to the National Center for Research on Earthquake Engineering for providing shaking table testing data.

REFERENCES

1. Ibrahim SR, Mikulcik EC. A time domain modal vibration test technique. *Shock and Vibration Bulletin* 1973; **43**(4):21–37.
2. Huang CS, Yang YB, Lu LY, Chen CH. Dynamic testing and system identification of a multi-span highway bridge. *Earthquake Engineering and Structural Dynamics* 1999; **28**:857–878.
3. Yong LP, Mickleborough NC. Modal identification of vibrating structures using ARMA model. *Journal of Engineering Mechanics ASCE* 1989; **115**:2232–2250.
4. Kadakal U, Yuzugullu O. A comparative study on the identification methods for the auto-regressive modeling from the ambient vibration records. *Soil Dynamics and Earthquake Engineering* 1996; **15**:45–49.
5. Loh CH, Wu TS. Identification of Fei-Tsui arch dam from both ambient and seismic response data. *Soil Dynamics and Earthquake Engineering* 1996; **15**:465–483.
6. Huang CS. Structural Identification from ambient vibration measurement using the multivariate AR model. *Journal of Sound and Vibration* 2000; **241**(3):337–359.
7. Rao BD, Arun KS. Model based processing of signals: a state space approach. *Proceedings of the IEEE* 1992; **80**(2):283–309.
8. VanDerVeen A, Deprettere EF, Swindlehurst AL. Subspace-based signal analysis using singular value decomposition. *Proceedings of the IEEE* 1993; **81**(9):1277–1308.
9. Viberg M. Subspace-based methods for the identification of linear time-invariant systems. *Automatica* 1995; **31**(12):1835–1851.
10. Juang J, Pappa R. An eigensystem realization algorithm for modal parameter identification and model reduction. *Journal of Guidance Control, and Dynamics* 1985; **8**:620–627.
11. Ljung L. *System Identification*: *Theory for the User*. Prentice-Hall: Englewood Cliff, NJ, 1987.
12. Ljung L. A simple start-up procedure for canonical form state space identification. *Proceedings of 30th IEEE Conference on Decision and Control*, Brighton, U.K., 1991; 1333–1336.
13. Gopinath B. On the identification of linear time-invariant systems from input–output data. *Bell System Technique Journal* 1969; **48**:1101–1113.
14. Moonen M, Moor BD, Vandenberghe L, Vandewalle J. On- and off-line identification of linear state-space models. *International Journal of Control* 1989; **49**:219–232.
15. Verhaegen M. Identification of the deterministic part of MIMO state space models given in innovations form from input–output data. *Automatica* 1994; **30**:61–74.
16. VanOverschcee P, DeMoor B. N4SID: subspace algorithms for the identification of combined deterministic-stochastic systems. *Automatica* 1994; **30**:75–93.
17. Viberg M, Wahlberg B, Ottersten B. Analysis of state space system identification methods based on instrumental variables and subspace fitting. *Automatica* 1997; **33**(9):1603–1616.
18. VanOverschee P, DeMoor B. Choice of state-space basis in combined deterministic-stochastic subspace identification. *Automatica*, *Special Issue Trends System Identification* 1995; **31**:1877–1884.

19. VanOverschee P, DeMoor B. *Subspace Identification of Linear Systems*: *Theory*, *Implementation*, *Applications*. Kluwer Academic Publishers: Dordrecht, 1996.
20. Huang CS. Modal identification of structures using ARMAV model for ambient vibration measurement. *Proceedings of 12th World Conference on Earthquake Engineering*, paper no. 1702/6/A, 2000.
21. Yeh SC, Cheng CP, Loh CH. Shaking table tests on scaled down five-storey steel structures. *NCREE Report No. NCREE-99-002*, *National Center for Research on Earthquake Engineering*, R.O.C., 1999 (in Chinese).
22. Allemang RL, Brown DL. A correlation coefficient for modal vector analysis. *Proceeding of the First International Model Analysis Conference*, Bethel, Connecticut, U.S.A., 1983; 110–116.
23. Lieven NAJ, Ewins DJ. Spatial correlation of mode shapes, the coordinate modal assurance criterion (COMAC). *Proceeding of the Sixth International Modal Analysis Conference*, 1988; 690–695.

